

MALAYSIAN JOURNAL OF ANALYTICAL SCIENCES

Journal homepage: https://mjas.analis.com.my/



Research Article

Technische universiteit Delft-1-supported nickel oxide doped-titanium dioxide for oxidative removal of methylene blue

Ling Shing Liau¹, Chui Min Ling¹, Sie-Tiong Ha², Nursyafreena Attan¹, and Siew Ling Lee^{1,3*}

¹Department of Chemistry, Faculty of Science, Universiti Teknologi Malaysia, 81310 Johor Bahru, Malaysia ²Faculty of Science, Universiti Tunku Abdul Rahman, Jln Universiti, Bandar Barat, 31900 Kampar, Perak, Malaysia ³Centre for Sustainable Nanomaterials, Ibnu Sina Institute for Scientific and Industrial Research, Universiti Teknologi Malaysia, 81310 Johor Bahru, Malaysia

*Corresponding author: lsling@utm.my

Received: 14 April 2025; Revised: 15 July 2025; Accepted: 22 July 2025; Published: 26 August 2025

Abstract

The elimination of organic dyes from wastewater is essential for mitigating environmental pollution. Conventional treatment methods often fail to completely remove these persistent pollutants. Among advanced oxidation processes, the Fenton-like reaction has garnered considerable attention for its effectiveness in dye degradation. This study reports the synthesis of Technische Universiteit Delft-1 (TUD-1) supported nickel oxide-doped titanium dioxide (NiO-TiO₂/TUD-1) as a Fenton-like catalyst for methylene blue (MB) removal. The catalysts were characterized using X-ray diffraction (XRD), Fourier Transform Infrared (FTIR) spectroscopy, ultraviolet-visible diffuse reflectance spectroscopy (UV-vis DRS), nitrogen adsorption-desorption analysis, and point of zero charge (pH_{PZC}). The results confirmed the presence of the anatase TiO₂ phase, successful NiO doping, and the incorporation of Ti species into TUD-1. Among the catalysts, 0.4 mol% NiO-TiO₂/TUD-1 exhibited the highest MB removal efficiency (91.8%) at pH 12 under dark conditions within 2 hours. Its catalytic activity was approximately 2.5 times higher than that of unsupported NiO-TiO₂. This performance is attributed to its high surface area (323 m²/g), mesoporous structure (~12 nm), and strong adsorption capacity (10.5 mg/g), which enhance dye uptake. The catalyst functions through a Ti⁴⁺/Ti³⁺ Fenton-like mechanism, reacting with hydrogen peroxide (H₂O₂) to generate hydroxyl radicals (•OH) that degrade MB. This catalyst demonstrates strong potential as a light-free solution for practical wastewater treatment.

Keywords: Fenton-like process, oxidative catalyst, TUD-1, titanium dioxide, nickel oxide

Introduction

In recent years, a growing concern has arisen over the discharge of organic dyes, particularly from the textile and paint industries, which negatively affect global water quality. These dyes are often toxic, carcinogenic, and chemically stable in aquatic environments, posing serious threats to ecosystems and human health [1, 2]. Among these dyes, methylene blue (MB), a widely used synthetic dye, is frequently detected in industrial wastewater. Its persistence and toxicity make it an urgent target for effective removal technologies. Thus, various conventional methods have been applied for MB removal, including physical, biological, and chemical processes such as adsorption, chemical reduction, and microbial treatment [3, 4]. Nevertheless, these approaches often suffer from several limitations, including high costs, pH dependence, high energy, and time consumption, as well as the generation of secondary waste [5, 6]. Furthermore, many of these methods merely transfer pollutants from one phase to

another rather than achieving complete degradation, necessitating further treatment steps [7, 8].

To overcome these challenges, advanced oxidation processes (AOPs) have been widely explored [9]. AOPs generate highly reactive species such as hydroxyl radicals (•OH), which can degrade refractory organic compounds into low or non-toxic small molecules [10, 11]. These methods are favored for their high degradation efficiency, fast reaction rates, and low generation of secondary pollutants [12]. Several AOPs have been developed, including photocatalysis, Fenton oxidation, ozone oxidation, and more. Among these, the Fenton process, based on the reaction between ferrous ions (Fe²⁺) and hydrogen peroxide (H₂O₂), has gained significant interest due to its simplicity, cost-effectiveness, and ability to operate under ambient conditions [13]. However, the conventional Fenton process is limited by a narrow pH range (2.8 - 3.5) and generates iron sludge, which

complicates catalyst recovery [10]. To address these drawbacks, Fenton-like systems have been developed using heterogeneous catalyst configurations that facilitate easier recovery and reuse [13]. Recent studies have shown that heterogeneous Fenton-like catalysts, such as modified titanium dioxide (TiO₂), can operate effectively across a broader pH range, thereby expanding the scope of AOP applications [14].

TiO₂ catalysts have generally been used for organic pollutant removal and wastewater treatment [15]. TiO₂ has gained significant interest for use as a catalyst due to its environmentally friendly characteristic, chemical stability, cost-effectiveness, and abundance [16, 17]. The anatase phase of TiO₂ is particularly desirable as it offers a relatively higher surface area, porosity, and adsorption capacity compared to the rutile phase, resulting in improved catalytic activity [18]. Nevertheless, TiO₂ is less effective for prolonged reactions due to the limited specific surface area and number of active sites, which reduces its long-term catalytic efficiency [19]. To overcome the limitations associated with the low surface area and limited active sites of TiO2, surface modification has emerged as a key strategy to enhance its catalytic efficiency. One effective approach involves doping TiO2 with suitable transition metal oxides to tailor its structural properties [20]. Among transition metal oxides, nickel oxide (NiO) stands out for its favorable optical properties, chemical stability, cost-effectiveness, and ease of synthesis, thus offering high catalytic activity and scalability for industrial applications [3]. Ni-based catalysts have been successfully applied in various catalytic processes, including dye degradation using oxidizing agents such as ozone [21]. In this study, NiO is incorporated as a dopant into TiO2 to address its inherent limitations. Doping TiO2 with NiO can increase the surface area and number of active sites and stabilize the anatase phase by preventing its transformation into rutile, thereby enhancing overall catalytic efficiency [16, 22].

In contrast, TiO₂ tends to aggregate due to its high surface energy, while excessive NiO loading can also lead to particle agglomeration [23]. Moreover, solid catalysts typically interact with dye molecules only on their surfaces, which limits the accessible active sites and results in relatively low catalytic activity [17]. Hence, various strategies have been explored to these problems, including address modification, the use of porous support materials, and more [24]. Among these, incorporating catalysts with support materials has become one of the most effective methods for dye removal from wastewater [9]. In this study, Technische Universiteit Delft-1 (TUD-1) was selected as the support material due to its unique properties. TUD-1 is a mesoporous silicate material that can be synthesized easily and functionalized with active sites in one pot via a nonsurfactant pathway [25, 26]. It features excellent

adsorption ability, large surface area, and a threedimensional open pore network, making it highly suitable for catalytic applications [27]. These structural characteristics enhance mass transfer and facilitate the uniform dispersion of active metal species within TUD-1 [28]. Its performance as a support material has been demonstrated in various applications, such as in the study by Alhanash [29], where Pt-TUD-1 outperformed other supports in cycloalkene hydrogenation due to enhanced accessibility and dispersion of active sites. These findings highlight the potential of TUD-1 as a robust and efficient support for transition metal catalysts. In the present study, TUD-1 was introduced to support NiO-TiO₂ in a Fenton-like catalytic system to enhance MB removal efficiency in wastewater treatment.

Building on this background, the present study introduces a novel NiO-doped TiO2 supported on (NiO-TiO₂/TUD-1) developed as TUD-1 heterogeneous Fenton-like system for MB removal from wastewater. This hybrid composite integrates the catalytic activities of NiO and TiO2 with the structural advantages of TUD-1, offering a synergistic system for efficient dye removal. To the best of our knowledge, this is the first report on synthesizing this composite methods, which combinational included precipitation, sol-gel method, wet-impregnation, and hydrothermal treatment. The effect of NiO doping concentrations on the physicochemical properties and catalytic activity of the composites was assessed through MB removal via adsorption and Fenton-like oxidative degradation under dark conditions with H₂O₂. By showing effective catalytic performance without light activation, this study presents a more energy-efficient and scalable alternative wastewater treatment using TiO2-based materials.

Materials and Methods Chemicals and reagents

Titanium(IV) isopropoxide (TTIP) (C₁₂H₂₈O₄Ti, 97%), nickel(II) nitrate hexahydrate (Ni(NO₃)₂.6H₂O), tetraethylammonium hydroxide (TEAOH) (C₈H₂₁NO₃, 35 wt.% in H₂O), and H₂O₂ (30%) were purchased from Sigma Aldrich Chemical Company. Meanwhile, absolute ethanol (C₂H₅OH) was obtained from Hayman Limited, whereas triethanolamine (TEA) (C₆H₁₅NO₃) was purchased from QRec Chemical Company. Tetraethyl orthosilicate (TEOS) (C₈H₂₀O₄Si) was acquired from Merck Chemical Company. All the chemicals and reagents were used as received without further purification.

Synthesis of TiO2 and NiO-TiO2 catalysts

TiO₂ was synthesized using a wet chemical precipitation approach, based on a previously reported procedure with minor modifications [23]. Initially, 6 mL of TTIP (2 M) was mixed with 10 mL of distilled water and stirred continuously for 45 minutes at 40°C. The resulting precipitate was then centrifuged and

washed several times with distilled water. Finally, the precipitate was dried at 90°C for 12 hours and then calcined at 500°C for 3 hours.

For NiO-TiO₂ synthesis, a similar procedure was followed using Ni(NO₃)₂.6H₂O as the nickel precursor. To prepare 1 mol% NiO-TiO₂, Ni(NO₃)₂.6H₂O was dissolved in distilled water and added to 2 M TTIP solution. The mixture was stirred for 80 minutes at 40°C, resulting in the formation of a pale-yellow precipitate. The precipitate was then centrifuged and washed several times with distilled water. Finally, it dried at 90°C for 12 hours and calcined at 500°C for 3 hours. The procedure was repeated to prepare other composites with x mol% NiO-TiO₂ (x = 0.2, 0.4, 0.6 and 0.8).

Synthesis of TUD-1 and TUD-1 supported NiO-TiO₂ catalysts

TUD-1 was prepared using the sol-gel method followed by hydrothermal treatment, according to a previous study from our research work with slight modification [23]. The molar composition used for TUD-1 synthesis was 1 TEOS: 0.5 TEA: 0.1 TEAOH: 11 H₂O. Initially, TEA was mixed with H₂O and stirred for 1 hour, followed by adding the mixture into TEOS. After stirring for 1 hour, TEAOH was added dropwise into the mixture and stirred for another 2 hours. The resulting mixture was aged at room temperature for 24 hours to form a solid gel. The solid gel was treated hydrothermally for 10 hours at 130°C and then dried at 100°C overnight. Finally, the resulting products were calcined at 600°C for 6 hours to obtain TUD-1.

x mol% NiO-TiO₂/TUD-1 composites (x = 0.2, 0.4, 0.6, 0.8 and 1.0) were synthesized using the same procedure as TUD-1, with a constant Si/Ti molar ratio of 30. Firstly, TEA was mixed with H₂O and stirred for 1 hour. In the meantime, pre-synthesized 1.0 mol% NiO-TiO₂ was mixed with TEOS and stirred for 1 hour. Next, the mixture of TEA and H₂O was added to the mixture of NiO-TiO₂ and TEOS and subsequently stirred for 2 hours. The resulting mixture was aged for 24 hours, followed by hydrothermal treatment at 130°C for 4 hours. The final product was dried at 100°C overnight and calcined at 600°C for 6 hours. The procedure was repeated to synthesize 0.2, 0.4, 0.6, and 0.8 mol% NiO-TiO₂/TUD-1 composites.

Characterization of catalysts

The physicochemical properties of TiO₂ and NiO-TiO₂/TUD-1 composites were characterized using several instruments. The phase purity and crystallinity of the composites were determined using powder X-ray diffraction (XRD) with a Rigaku SmartLab X-ray diffractometer. Fourier Transform Infrared (FTIR) spectroscopy was employed using Thermo Scientific Nicolet iS10 Spectrometer to identify the functional groups present in the composites. The optical information of the composites was examined using

ultraviolet-visible diffuse reflectance spectroscopy (UV-vis DRS) on a Shimadzu UV-3600 Plus spectrometer. The Brunauer-Emmett-Teller (BET) surface area, Barrett-Joyner-Halenda (BJH) pore size distribution, and pore volume were determined by N₂ adsorption-desorption analysis using a Thermo Fisher Scientific Sorptomatic 1990 surface analyzer.

Determination of point of zero charge (pH_{PZC})

The point of zero charge (pH_{PZC}) of the composites was identified using the salt addition approach with slight modifications [30]. Firstly, 10 mL of sodium chloride (NaCl) solution (0.1 M) was added to a 50 mL conical flask containing 50 mg of the composites. The initial pH (pH_i) of the solution was adjusted to pH 2 using dilute hydrochloric acid (HCl) and sodium hydroxide (NaOH) solutions. The mixture was then equilibrated for 24 hours at 200 rpm using a mechanical orbital shaker. The final pH (pH_f) of the solution was measured and recorded. The experiment was repeated with other pH_i values (pH 5, 7, 9, and 12). The difference between pH_i and pH_f was calculated and labeled as ΔpH . A plot of ΔpH versus pH_i was constructed and the intersection between the curve and X-axis was identified as pH_{PZC}.

Fenton-like oxidative catalytic performance of catalysts

The Fenton-like oxidative catalytic performance of the catalysts was assessed via the catalytic oxidation of MB in the presence of H₂O₂ as an oxidant under dark conditions to prevent the photocatalysis effect during the reaction. In each trial, 10 mg of the synthesized sample was added to 50 mL of MB solution (5 ppm) and stirred for 1 hour to reach adsorption equilibrium. Next, H₂O₂ (500 µL, 30% v/v) was added to initiate oxidative degradation. An aliquot of 10 mL of the mixture was withdrawn and centrifuged to separate the catalyst. The final concentration of the supernatant was determined using UV-vis spectroscopy. The final concentration of MB was calculated using Equation (1). Each experiment was repeated in triplicate for all catalysts. Control experiments containing only H₂O₂ and MB were also conducted.

Removal percentage of MB (%)
$$= \frac{C_0 - C_f}{C_0} \times 100\% = \frac{A_0 - A_f}{A_0} \times 100\% \tag{1}$$

where C_0 and A_0 are the initial concentration (mg/L) and absorbance (a.u.) of MB, and C_f and A_f are the final concentration (mg/L) and absorbance (a.u.), respectively.

Adsorption tests were employed to evaluate the capacity of the catalysts to adsorb MB. Each catalyst was tested for its adsorption ability over 1 hour at room temperature. The adsorption capacity (q_e) of the catalysts was calculated using Equation (2):

$$q_{e}\left(mg/g\right) = \frac{(C_{o} - C_{e})V}{W} \tag{2}$$

where C_o and C_e are the initial and equilibrium concentration of MB in solution (mg/L); V is the volume of solution (L) and W is the weight of the catalyst (g).

Optimization of oxidative catalytic performance of catalysts

The effects of pH and contact time were investigated to determine the optimal conditions for the oxidative catalytic performance of the catalysts. To investigate the effect of pH, the catalyst with the highest removal efficiency was added to 50 mL of MB solution (5 ppm) after the initial oxidative catalytic performance test. The pH of the solution was adjusted to pH 2 using HCl (1.0 M) and NaOH solution (1.0 M). The experiment followed the same procedure as described in the catalytic oxidative performance test. The experiment was repeated at different pH levels (5, 7, 9, and 12). To study the effect of contact time, the catalyst with the highest removal efficiency was applied to 50 mL of MB solution (5 ppm) at the optimal pH. The experiment was initially conducted for 1 hours to determine the removal efficiency of the catalyst. The experiment was then repeated at different contact times (1.5, 2.0, 2.5, and 3.0 hours).

Results and Discussion Structural analysis

TiO2, NiO-TiO2, TUD-1, and a series of NiO-TiO₂/TUD-1 were characterized via determination, FTIR spectroscopy, XRD, and UV-vis DRS. Figure 1 illustrates the XRD diffraction pattern of the synthesized catalysts (a) TiO2, (b) 1.0 mol% NiO-TiO₂, (c) TUD-1, (d) 0.4 mol% NiO-TiO₂/TUD-1, and (e) 1.0 mol% NiO-TiO₂/TUD-1. The XRD pattern proved that the synthesized pure TiO₂ exhibited a tetragonal anatase phase with distinct peaks at $2\theta = 25.24^{\circ}$, 37.82° , 47.99° , 53.92° , 55° , and 62.64°, corresponding to the (110), (004), (200), (105), (211) and (204) planes [31]. The synthesized TiO₂ showed an XRD pattern consistent with pure anatase TiO₂, as confirmed by the standard ICDD file number 21-1272. After doping with 1.0 mol% NiO, the anatase phase remained unchanged, and no additional peaks from NiO were observed, suggesting either low concentration or high dispersion of NiO within TiO₂. Meanwhile, the XRD pattern of TUD-1 displayed a broad hump around 22°, indicative of its amorphous nature [32]. Furthermore, the XRD patterns of 0.4 mol% and 1.0 mol% NiO-TiO₂/TUD-1 were like that of the anatase phase of TiO2. The crystallinity of TiO2 reduced notably with increasing NiO doping concentrations. This may be due to the reduced peak intensity of the anatase phase peak and inhibition of crystal grain growth, which could promote the formation of the amorphous phase [16].

Functional group analysis

Figure 2 illustrates the FTIR spectra of (a) TiO₂, (b) 1.0 mol% NiO-TiO₂, (c) TUD-1, (d) 0.2 mol% NiO-TiO₂/TUD-1, (e) 0.4 mol% NiO-TiO₂/TUD-1, (f) 0.6 mol% NiO-TiO₂/TUD-1, (g) 0.8 mol% NiO-TiO₂/TUD-1 and (h) 1.0 mol% NiO-TiO₂/TUD-1. For all samples, the prominent and distinctive bands observed in the regions of 3369 – 3475 cm⁻¹ and 1624 - 1647 cm⁻¹ indicate the O-H stretching vibration and O-H bending, respectively, confirming the presence of the hydroxyl group on the TiO₂ surface and facilitating the adsorption of MB on the catalyst surface [5]. Meanwhile, TiO2 and 1.0 mol% NiO-TiO2 exhibited a broad band in the range of $400 - 800 \text{ cm}^{-1}$, suggesting the presence of Ti-O-Ti stretching vibration [8]. However, there is no distinct band from NiO due to the low mole percentage of NiO doping [33]. In addition, TUD-1 and TUD-1 supported catalysts exhibited significant bands such as Si-O-Si asymmetric stretching (1099 – 1115 cm⁻¹), symmetric stretching $(798 - 806 \text{ cm}^{-1})$, bending $(465 - 467 \text{ cm}^{-1})$, respectively, confirming the incorporation of the silica framework of TUD-1 in the TUD-1 supported catalysts. Furthermore, Si-O-Ti stretching (970 – 975 cm⁻¹) was detected, which explains the successful incorporation of Ti species into the silica framework of TUD-1 [34].

UV-vis DRS analysis of Ti species coordination

The UV-vis DRS spectra of the synthesized catalysts are depicted in Figure 3. UV-vis DRS analysis was conducted to determine the form of Ti species present in the catalysts, following the approach of Klinyod [35], who used this technique to confirm the structure of isomorphically substituted Ti(IV) sites within the support framework. The absorption peak at 235 – 244 nm corresponds to charge transfer from O2- to Ti4+, indicating the presence of tetrahedrally coordinated Ti species [24]. These tetrahedral Ti species are widely recognized as the most catalytically active sites in oxidation reactions [36]. However, their intensity decreases with increasing NiO loading. In contrast, the absorption peak at 283 - 295 nm corresponds to octahedrally coordinated Ti species, and its intensity increases with NiO loading [36, 37]. This confirms the coexistence of both tetrahedral and octahedral Ti species in the synthesized catalyst. Besides, UV-vis DRS was further used to verify the successful doping of NiO into TiO2, as evidenced by a red shift in the absorption edge for the 1.0 mol% NiO-TiO₂ sample [38]. A similar observation was reported by Guettaia [39], where UV-vis DRS confirmed the coordination of iron within the TUD-1. In this study, the red shift observed in the absorption spectrum serves as indirect evidence of compositional and structural changes in the sample. Other characterization techniques, such as XRD and FTIR, were unable to detect NiO in the composites, likely due to its low doping concentration.

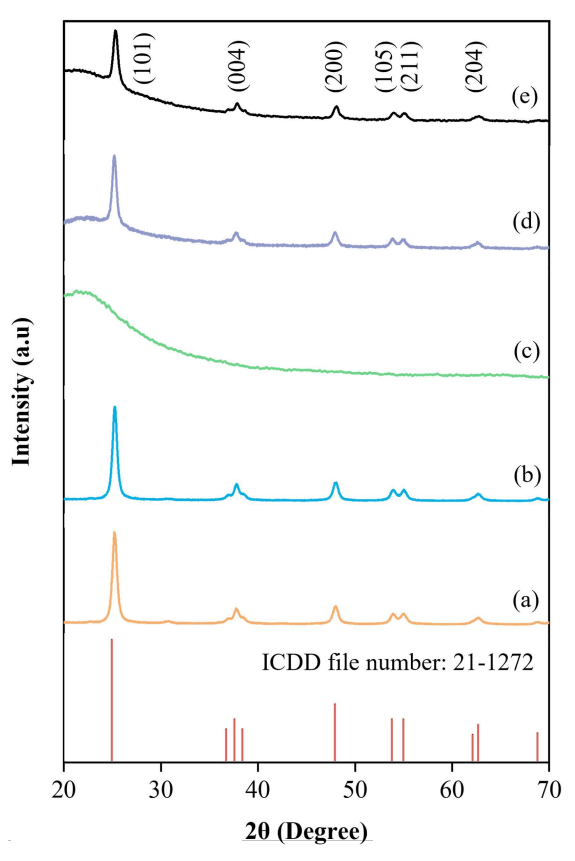


Figure 1. XRD patterns of (a) TiO_2 , (b) 1.0 mol% NiO- TiO_2 , (c) TUD-1, (d) 0.4 mol% and (e) 1.0 mol% NiO- TiO_2/TUD -1

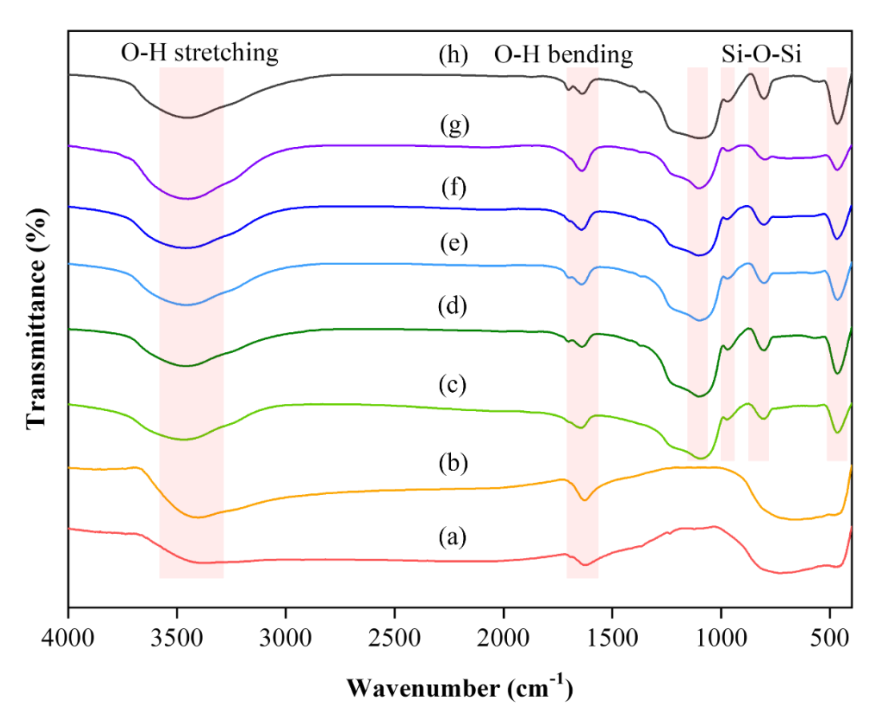


Figure 2. FTIR spectra of (a) TiO_2 , (b) 1.0 mol% $NiO-TiO_2$, (c) TUD-1, (d) 0.2 mol% $NiO-TiO_2/TUD-1$, (e) 0.4 mol% $NiO-TiO_2/TUD-1$, (f) 0.6 mol% $NiO-TiO_2/TUD-1$, (g) 0.8 mol% $NiO-TiO_2/TUD-1$ and (h) 1.0 mol% $NiO-TiO_2/TUD-1$

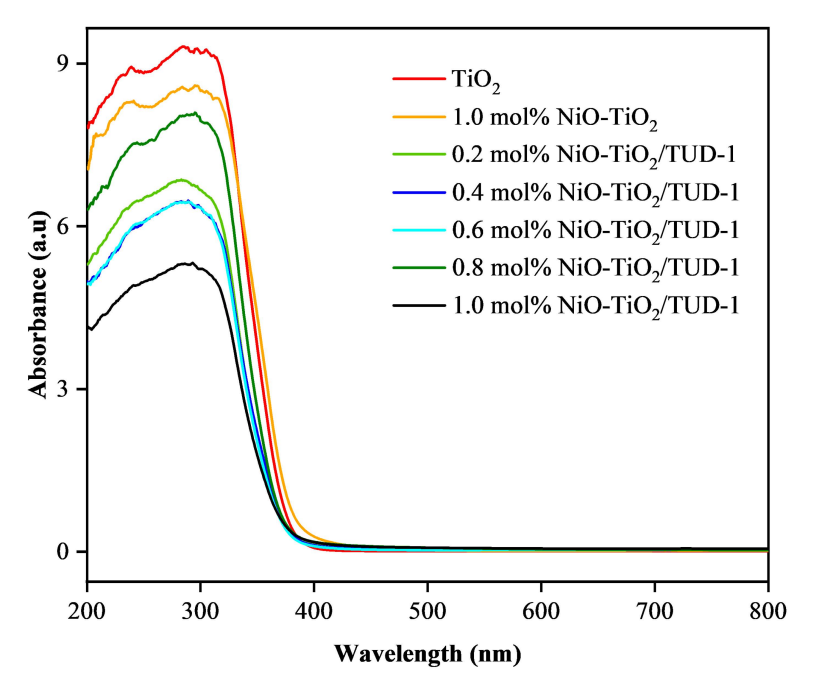


Figure 3. UV-vis DRS spectra of TiO₂, 1.0 mol% NiO-TiO₂ and NiO-TiO₂/TUD-1 composites

Surface area and porosity analyses

The surface area and porosity properties of the synthesized catalysts were determined through nitrogen adsorption-desorption analysis. The textural data, including surface area, pore volume, and pore size of the catalysts, are tabulated in **Table 1**.

Surface area, pore volume, and pore size distribution are usually the key parameters influencing dye removal efficiency [40]. As shown in Table 1, TUD-1 exhibits the highest surface area of 924 m²/g. The surface areas of the NiO-TiO2 incorporating with TUD-1 are significantly larger than that of pure TiO₂, exceeding 300 m²/g. The pore diameters of the composites range from 11.77 to 12.29 nm, confirming their mesoporous nature. A slight decrease in BET surface area and pore volume is observed as the NiO doping concentrations increase from 0.2 mol% to 1.0 mol%. Among the samples, 0.4 mol% NiO-TiO₂/TUD-1 exhibited the highest surface area (323 m²/g) and a mesoporous structure with an average pore size of approximately 12 nm. These characteristics facilitate the simultaneous adsorption of MB and its

subsequent catalytic oxidation, hence enhancing dye removal efficiency. The increased surface area and porosity provide more active sites and promote efficient diffusion of dye molecules and oxidants, thus promoting catalytic degradation [41].

The N₂ adsorption-desorption isotherms of TiO₂ and with NiO-TiO₂/TUD-1 varying NiO concentrations are illustrated in **Figure 4**. All samples exhibited type IV isotherms, indicating the presence of mesoporous structures based on IUPAC classification. From the isotherm curve, it was observed that TiO₂ has H2 hysteresis loops, indicating the presence of bottleneck-shaped pores. The ink-bottle pores with narrow necks may hinder molecular diffusion and limit dye removal efficiency. In contrast, with increasing NiO doping, the hysteresis loops transitioned to H1 type in the 0.2, 0.4, and 1.0 mol% NiO-TiO₂/TUD-1 samples. The appearance of H1 type denotes the formation of cylindrical-shaped pores, which facilitate the effective diffusion of MB and H₂O₂ into active sites, thus enhancing both adsorption and catalytic degradation.

Table 1. Textural properties of the catalysts

Samples	Surface area (m²/g)	Pore volume (cm ³ /g)	Pore size (nm)
TiO ₂	61	0.22	14.57
TUD-1*	924	0.69	2.83
0.2 mol% NiO-TiO ₂ /TUD-1	322	0.99	12.29
0.4 mol% NiO-TiO ₂ /TUD-1	323	0.97	12.06
1.0 mol% NiO-TiO ₂ /TUD-1	303	0.89	11.77

^{*}Data adapted from [23]

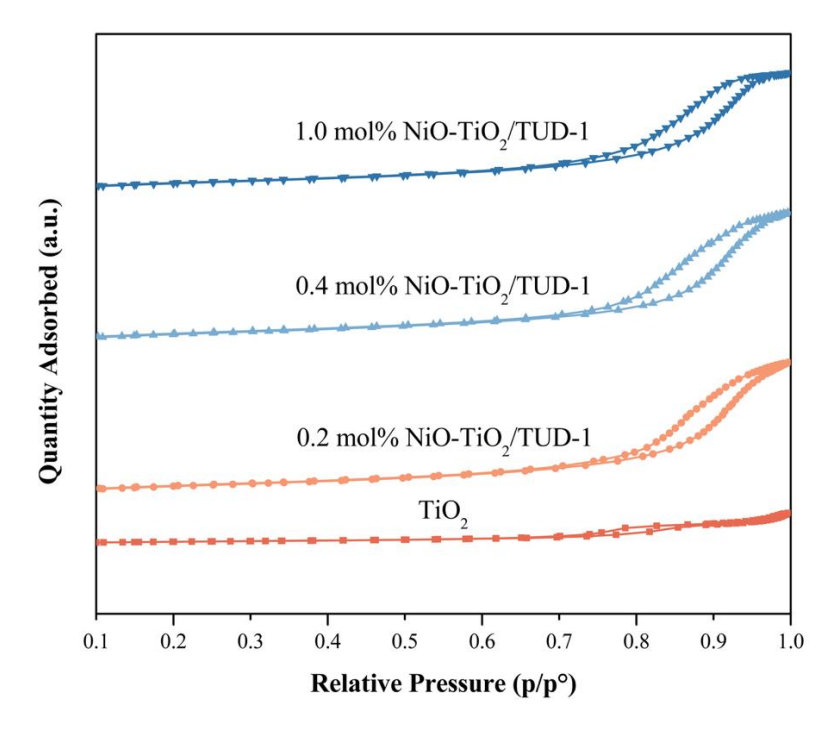


Figure 4. N₂ adsorption-desorption isotherms of TiO₂ and x mol% NiO-TiO₂/TUD-1 (x = 0.2, 0.4 and 1.0)

Surface charge analysis

The relative surface charge of the catalyst was investigated by determining its pH_{PZC} to study the electrostatic interactions between cationic dye molecules and the catalyst surface. **Figure 5** illustrates the pH_{PZC} determination curve of 0.4 mol% NiO-TiO₂/TUD-1 catalyst, plotted as ΔpH versus $pH_{initial}$. As shown in **Figure 5**, the pH_{PZC} of 0.4 mol% NiO-TiO₂/TUD-1 is 4.16, based on the intersection point with the X-axis. At the pH of 4.16, 0.4 mol% NiO-TiO₂/TUD-1 exhibited a neutral surface charge. Below pH 4.16, the catalyst surface is positively charged, while above this pH, it becomes negatively charged.

Adsorption and oxidative catalytic performance of catalysts

The oxidative catalytic performance of the synthesized catalysts was evaluated through the catalytic oxidative removal of MB in the presence of H₂O₂. Before the oxidative degradation reaction, an adsorption test was conducted under dark without the presence of H₂O₂. The degradation experiment was also performed under dark in the presence of H₂O₂ to eliminate the influence of photocatalytic effect by the NiO-TiO₂/TUD-1 composites. A control experiment using only H₂O₂ and without any catalyst was conducted for comparison. The adsorption capacity of the catalysts was evaluated after one hour of adsorption testing at room temperature. The adsorption capacities of the catalysts are illustrated in **Figure 6**.

As shown in **Figure 6**, the 0.4 mol% NiO-TiO₂/TUD-1 exhibited the highest adsorption capacity of 10.5 mg/g. This suggests that the catalyst effectively enhances MB removal, primarily due to strong adsorption affinity and high surface area, which increase the accessibility of MB molecules to reactive species during oxidative degradation. Adsorption increases the concentration of reactant molecules on the catalyst surface; the catalyst and elements undergo collision with each other to yield an activated complex [9]. Therefore, the activated complex decomposes to yield a product and catalyst. This makes it easy to separate the catalyst after the adsorption process [9]. Notably, samples with NiO loading of 0.6 mol% and above showed a decline in qe, with 1.0 mol% NiO-TiO₂/TUD-1 recording only 6.2 mg/g. This decline is likely due to NiO agglomeration at higher concentrations, which reduces the available surface area and active sites. Conversely, the significant increase in qe from TiO₂ (1.1 mg/g) to 0.2 mol% NiO-TiO₂/TUD-1 (6.5 mg/g) highlights the positive contribution of the TUD-1 support in enhancing surface adsorption.

The MB removal efficiency of all catalysts was evaluated and is illustrated in **Figure 7**. The removal efficiency was calculated based on the UV-vis absorbance at $\lambda = 664$ nm, with a constant initial MB concentration of 5 ppm and 500 μL of H_2O_2 over 2 hours.

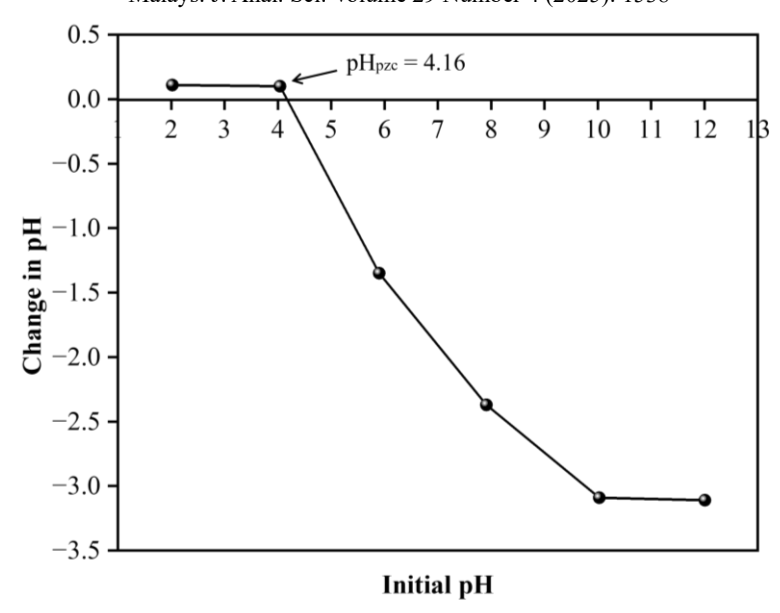


Figure 5. pH_{PZC} determination curve of 0.4 mol% NiO-TiO₂/TUD-1 composite

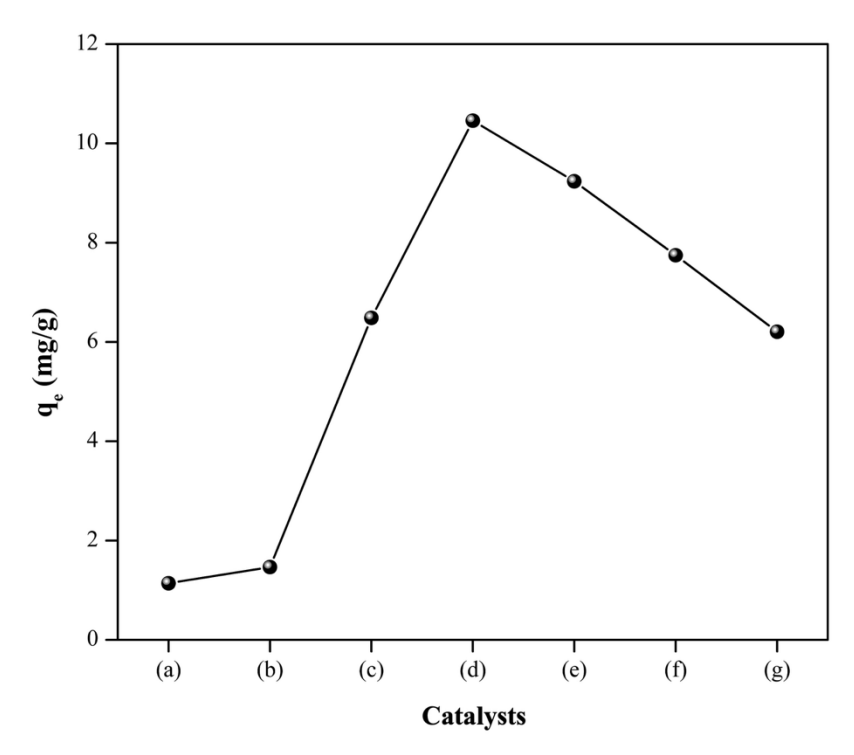


Figure 6. Adsorption capacity of (a) TiO_2 , (b) 1.0 mol% $NiO-TiO_2$, (c) 0.2 mol% $NiO-TiO_2/TUD-1$, (d) 0.4 mol% $NiO-TiO_2/TUD-1$, (e) 0.6 mol% $NiO-TiO_2/TUD-1$, (f) 0.8 mol% $NiO-TiO_2/TUD-1$ and (g) 1.0 mol% $NiO-TiO_2/TUD-1$

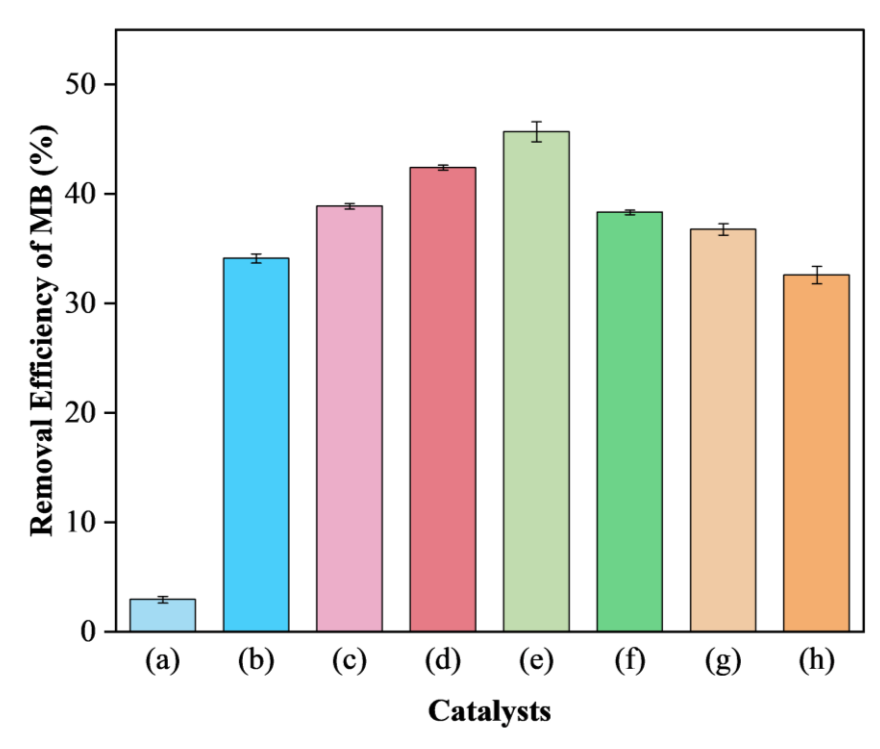


Figure 7. Removal efficiency of MB using (a) H₂O₂, and H₂O₂ with (b) TiO₂, (c) 1.0 mol% NiO-TiO₂, (d) 0.2 mol% NiO-TiO₂/TUD-1, (e) 0.4 mol% NiO-TiO₂/TUD-1, (f) 0.6 mol% NiO-TiO₂/TUD-1, (g) 0.8 mol% NiO-TiO₂/TUD-1 and (h) 1.0 mol% NiO-TiO₂/TUD-1

The control experiment using only H₂O₂ showed the lowest MB removal efficiency (2.9%). The low efficiency is attributed to the oxidizing nature of H₂O₂ alone, which lacks sufficient catalytic activation. This finding agrees with previous studies, which claimed that H₂O₂ requires catalyst activation for the effective oxidation of MB [42, 43]. The MB removal efficiency of TiO₂ with H₂O₂ was 34.1%, likely due to the generation of HOO• and •OH radicals upon its interaction with H₂O₂, which improved the degradation efficiency of MB [44].

The 1.0 mol% NiO-TiO2 catalyst achieved removal efficiency of 37.6%, a 3.5% increase over TiO₂, attributed to the increased surface area resulting from NiO doping [16]. However, the improvement was constrained by the cationic nature of MB, which reduces its affinity for the interaction between Ni⁺ ions on the catalyst surface [45]. It was previously reported that the TUD-1 showed negligible catalytic activity due to limited active sites, even though it has a relatively large surface area and pore volume as compared to other prepared samples [23]. Meanwhile, 0.2 mol% NiO-TiO₂/TUD-1 achieved a removal efficiency of 42.3%, which increased by about 5%. It is documented that the large surface area of TUD-1 could increase the adsorption ability and thus improve the catalytic activity in MB degradation [46, 47].

As shown in **Figure 7**, it can be noticed that the MB removal efficiency of 0.4 mol% NiO-TiO₂/TUD-1 was the highest (45.7%), which is consistent with its

highest adsorption capacity. It has been widely accepted that the increased dopant concentration enhances the adsorption capability and improves accessible surface area of the doped catalysts. Furthermore, the uniform distribution of NiO dopants on TiO₂ also contributed to the improved removal efficiency of the catalyst [18]. It has been found that NiO-TiO₂ composites were able to exert a significant cooperative influence when incorporated into TUD-1 support materials. With an optimal and appropriate concentration of 0.4 mol% NiO, the catalyst was significantly improved in terms of its performance, which made it an excellent candidate for the removal of MB from an aqueous solution.

In contrast, increasing the NiO dopant concentration from 0.6 to 1.0 mol% resulted in a decrease in MB removal efficiency. This decline may be due to excessive NiO loading, which cause dopants agglomeration or reduces the active surface area of catalyst [18]. These findings align with previous research indicating that a high dopant concentration can cause agglomeration on TiO₂, leading to decrease in the crystallite size and catalytic activity [16]. Consequently, decrease in specific surface area reduces the catalyst's MB adsorption capability, ultimately diminishing its oxidative degradation efficiency.

Method optimization

0.4 mol% NiO-TiO₂/TUD-1 catalyst was chosen for the optimization method since it exhibits the highest

efficiency of MB removal. A series of MB solutions loaded with 0.4 mol% NiO-TiO₂/TUD-1 were prepared and employed for the investigation of optimal conditions for MB removal methods. The parameters involved are the pH of the MB solution (pH 2, 5, 7, 9, and 12) and contact time (1.0, 1.5, 2.0, 2.5, and 3.0 hours). A one-variable-at-a-time method was used for the optimization of the parameters.

Effect of pH

The adsorption of MB dye on the catalyst surface significantly influenced removal efficiency, as did the pH of the dye solution, which played a crucial role in the catalytic and oxidative degradation of the dye solution [48]. Therefore, a range of pH levels from 2 to 12 was tested to determine the pH effect on the MB removal efficiency. **Figure 8(a)** illustrates the removal efficiency of MB by 0.4 mol% NiO-TiO₂/TUD-1 at different pH values, with a constant initial concentration of MB and volume of H₂O₂, over a 2-hour reaction time.

The highest MB removal efficiency was achieved at pH 12 with a removal efficiency of 91.9%, followed by 75.7% at pH 9. At neutral pH 7, the efficiency dropped significantly to 43.3%. The efficiency of MB removal decreased to 39.3% at pH 5 and 26.7% at pH 2, which are acidic conditions. It could be observed that the MB removal efficiency at pH 12 exhibited a 2-fold improvement over pH 7, indicating that the MB removal efficiency increased as the pH of the MB solution increased. This finding was also in agreement with previous work on degradation efficiency [48].

As for the adsorption, it is primarily a result of the electrostatic attraction between positively charged MB and 0.4 mol% NiO-TiO₂/TUD-1, since MB is a cationic dye that carries a positive charge in solution [49]. The pH_{PZC} of 0.4 mol% NiO-TiO₂/TUD-1 was determined to be 4.16. The catalyst surface was negatively charged at neutral and alkaline pH and thus attracted the positively charged MB molecules. Therefore, as the solution pH increases, the catalyst surface becomes more negatively charged, enhancing its adsorption capacity. In contrast, under acidic conditions, electrostatic repulsion limits the adsorption of MB on the catalyst surface. This behavior is consistent with previous findings [50].

As part of catalytic oxidative degradation, highly reactive radicals were produced from H₂O₂, which react with MB [51]. Per literature reports, •OH radical are generated when Ti⁴⁺ on the catalyst surface interact with H₂O₂ [44]. Therefore, it can be concluded that the nature of the catalytic reaction, the properties of the targeted pollutant, and its adsorption capacity on the catalyst surface all have significant impacts on the effectiveness of the oxidative degradation and adsorption process [49].

Effect of contact time

The effect of contact time on the MB removal was investigated using 0.4 mol% NiO-TiO₂/TUD-1 under optimal pH condition (pH 12) with a constant initial MB concentration and fixed H₂O₂ volume. Figure 8(b) illustrates the removal efficiency of MB by using 0.4 mol% NiO-TiO₂/TUD-1 at different contact times. Without H₂O₂, the removal efficiency of MB was 80.5%, indicating relatively high MB adsorption efficiency due to the abundance of unoccupied active sites on the catalyst surface, which allow easy access for MB molecules [52]. In the presence of H₂O₂, the MB removal efficiency increased to 86.9% after 1.5 hours and reached a maximum of 91.8% after 2 hours. This indicated that the contact time of 2 hours provided a sufficient duration for the optimal adsorption and catalytic degradation of MB [53].

However, the removal efficiency reduced to 83.9% after 2.5 hours. This reduction may be due to the decreased availability of active sites and increased repulsive interaction between MB molecules in solution and those already adsorbed [52]. In addition, the effectiveness of catalytic oxidative degradation may diminish over time as $\rm H_2O_2$ is gradually consumed during the reaction. After 3 hours, the removal efficiency was constant at 83.6%, suggesting that equilibrium has been achieved on the catalyst surface and thus limiting further MB removal.

Some NiO-TiO₂ related catalysts have been reported, and the findings are summarized in **Table 2**. The reaction parameters, such as light source, irradiation time, mass of catalyst loading, and H₂O₂ loading amount, have been investigated in this work and other research. Obviously, the synthesized NiO-TiO₂/TUD-1 catalyst has promising potential for the catalytic degradation of aqueous MB.

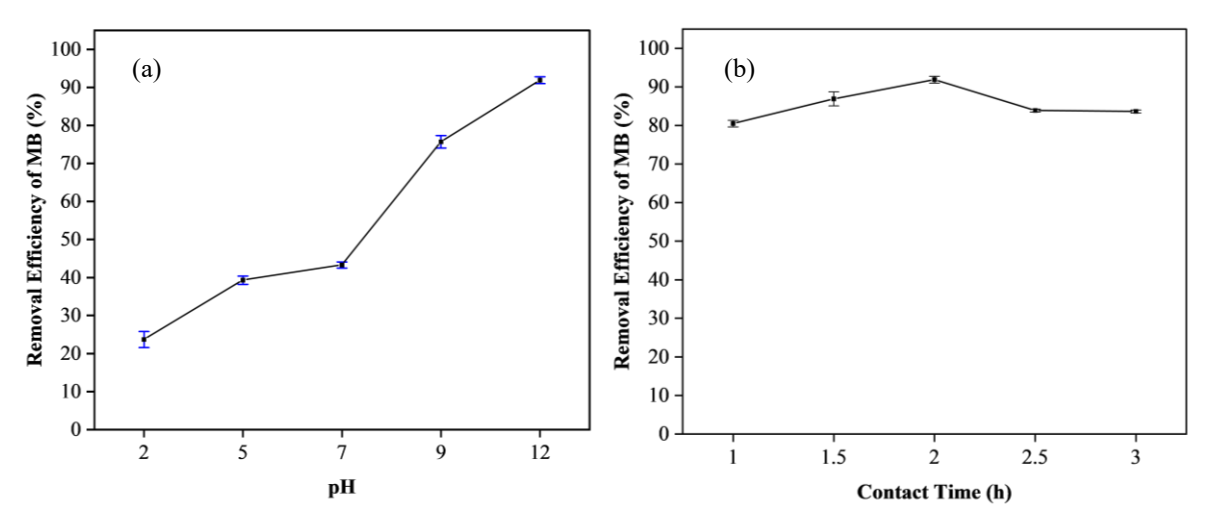


Figure 8. Effects of (a) pH of MB solution; (b) contact time on the removal efficiency of MB

Table 2. Performance comparison of some NiO-TiO2 related catalysts for the removal of aqueous MB solution

Catalyst	Reaction Conditions	Catalyst Dosage	Mechanism	Removal Efficiency	Reference
NiO-TiO ₂	Concentration: 5 mg/L in 25 mL Light source: Visible light Reaction time: 20 minutes	100 mg	Photodegradation	TiO ₂ : 30% degradation NiO-TiO ₂ : 80.63% degradation	[54]
NiO- TiO ₂ /TUD-1	Concentration: 5 mg/L in 50 mL Light source: No Reaction time: 120 minutes H ₂ O ₂ amount: 0.5 mL (30%	10 mg	Adsorption and oxidative degradation	TiO ₂ : 34.1% degradation NiO-TiO ₂ /TUD-1: 91.90% degradation	This study
NiO/Ag/TiO ₂	Concentration: 5 mg/L in 80 mL Light source: Visible light Reaction time: 60 minutes	80 mg	Adsorption and photodegradation	TiO ₂ : 60.7% degradation NiO/Ag/TiO ₂ : 93.15% degradation TiO ₂ : 67.30%	[55]
Ni-TiO ₂ thin film	Concentration: 3 mg/L in 5 mL Light source: UV light Reaction time: 360 minutes	Not mentioned	Photodegradation	degradation NiO-TiO ₂ thin film: 75.83% degradation	[56]
TiO ₂ /NiO	Concentration: 5×10^{-5} mol/L in 5 mL Light source: UV light Reaction time: 60 minutes	100 mg/L	Photodegradation	TiO ₂ : 62.4% degradation TiO ₂ /NiO: 98.3% degradation	[57]
NiO ₂ /TiO ₂	Concentration: 2 µmolL ⁻¹ in 50 mL Light source: UV-A light Reaction time: 60 minutes	Not mentioned	Adsorption and photodegradation	TiO ₂ : 5.8% degradation TiO ₂ /NiO: 25.3% degradation	[58]

Proposed mechanism

The removal of MB using NiO-TiO₂/TUD-1 in the presence of H₂O₂ involves two main steps. Step one involves the adsorption of oxidized MB molecules (MB•⁺) onto the catalyst surface [59]. The introduction of H₂O₂ would favor the adsorption of MB on catalyst surface due to the generation of superoxide anions (O₂·) in the cationic MB solution, which could alter the surface charge of the catalysts and thus enhance the adsorption of MB. Furthermore, due to the high surface area of NiO-TiO₂/TUD-1, MB molecules are efficiently adsorbed onto its surface.

Step two involves the oxidative degradation of MB via reactive oxidative species (ROS), primarily O₂-•/•OOH and •OH. The presence of H₂O₂ initiates the generation of ROS and accelerates MB degradation by breaking down MB molecules [60]. In the NiO-TiO₂/TUD-1 catalyst system, Ti⁴⁺ sites on the catalyst surface interact with H₂O₂ to form surface-bound complexes that facilitate radical generation. Radical adsorption, such as superoxide radical anions, may bind to the surface, resulting in a more negative surface potential, which promotes the adsorption of cationic dyes. Furthermore, the oxidative environment created at the surface of the solid-liquid interface may

facilitate the subsequent degradation of adsorbed MB. Moreover, the NiO dopant is involved in the MB degradation in the presence of the oxidant, such as H_2O_2 , where the NiO dopant could be used in the production of reactive oxidizing agent radicals, singlet oxygen (1O_2) [61].

The mechanism of the MB removal using NiO-TiO₂/TUD-1 in the presence of H_2O_2 is proposed by Equations (3) to (8) [62]. The process begins with surface adsorption of MB with the catalyst (Equation 3). The redox-active Ti species (Ti³⁺/Ti⁴⁺) then catalyze the decomposition of H_2O_2 to produce highly reactive •OOH, •OH, O_2 - and 1O_2 radicals via the indirect oxidation processes (Equations 4 to 7). These •OOH, •OH, O_2 - and 1O_2 radicals, which dominate the degradation process, subsequently attack the adsorbed MB molecules (Equation 8).

Step 1: Adsorption of MB

 $MB + NiO-TiO_2/TUD-1 \rightarrow MB@NiO-TiO_2/TUD-1$

(3)

(8)

Step 2: Oxidative degradation via ROS

$$Ti^{4+} + H_2O_2 \rightarrow Ti^{3+} + O_2^{-} + 2H^+$$
(4)

$$O_2^{-} + H_2O \rightarrow \bullet OH + H_2O_2$$
(5)

$$Ti^{3+} + H_2O_2 \rightarrow Ti^{4+} + O_2^{-} + \bullet OH + {}^{1}O_2$$
(6)

 $MB-H_2O_2 \rightleftharpoons Reaction intermediate + •OOH + O_2$ (7)

MB@ NiO-TiO₂/TUD-1@ $H_2O_2 \rightarrow$ Reaction intermediates/ NiO-TiO₂/TUD-1 + $H_2O + O_2$

Conclusion

A series of NiO₂-TiO₂/TUD-1 catalysts was successfully synthesized with different doping ratios of NiO (0.2, 0.4, 0.6, 0.8, and 1.0 mol%). The catalyst was evaluated for the combination adsorption and Fenton-like oxidative degradation of MB under dark conditions using H₂O₂ as the oxidant. The characterization results demonstrated the incorporation of Ti species into the TUD-1, the presence of the anatase phase, both tetrahedral and octahedral Ti species, successful NiO doping, and a desirable mesoporous structure with high surface areas. Furthermore, the use of TUD-1 support provided sufficient surface area for the removal of organic dye, enhancing the removal performance of the catalysts. Among the tested catalysts, 0.4 mol% NiO-TiO₂/TUD-1 exhibited the highest MB removal efficiency (91.8%) at pH 12 within 2 hours, increased about 2.5-fold compared to unsupported NiO-TiO₂. This superior performance is due to its enhanced adsorption capacity, high surface area (323 m²/g), mesoporous structure (~12 nm), and active Ti⁴⁺/Ti³⁺ redox sites that facilitate the ROS generation. The study shows that NiO-TiO₂/TUD-1 effectively integrates adsorption and oxidative degradation, enabling effective dye removal without the need for light activation. This energy-efficient catalyst holds

strong potential for practical wastewater treatment applications.

Acknowledgement

The authors would like to acknowledge the financial support obtained from the Ministry of Higher Education Malaysia (MOHE) and Universiti Teknologi Malaysia (UTM) through the Potential Academic Staff grant (Cost centre: QJ130000.2754.03K86). The authors are grateful to the University Industry Research Laboratory, UTM, for the research facilities, including the XRD.

References

- 1. Ma, D., Yi, H., Lai, C., Liu, X., Huo, X., An, Z., Li, L., Fu, Y., Li, B., Zhang, M., Qin, L., Liu, S., and Yang, L. (2021). Critical review of advanced oxidation processes in organic wastewater treatment. *Chemosphere*, 275: 130104.
- 2. Mohammed, H. A., Khaleefa, S. A., and Basheer, M. I. (2021). Photolysis of methylene blue using an advanced oxidation process (ultraviolet light and hydrogen peroxide). *Journal of Engineering and Sustainable Development*, 25(1): 59-67.
- Bui, B. C., Vu, N. N., Nemamcha, H. E., Nguyen, H. T., Nguyen, V. A., and Nguyen-Tri, P. (2025). Single nickel atoms doped into TiO₂ decorating carbon quantum dots for boosting photodegradation of ciprofloxacin. *Journal of Water Process Engineering*, 70: 106904.
- Santos, É. N., László, Z., Hodúr, C., Arthanareeswaran, G., and Veréb, G. (2020). Photocatalytic membrane filtration and its advantages over conventional approaches in the treatment of oily wastewater: A review. Asia-Pacific Journal of Chemical Engineering, 15(5): e2533.
- Fito, J., Abewaa, M., Mengistu, A., Angassa, K., Ambaye, A. D., Moyo, W., and Nkambule, T. (2023). Adsorption of methylene blue from textile industrial wastewater using activated carbon developed from *Rumex abyssinicus* plant. *Scientific Reports*, 13(1): 5427.
- Oladoye, P. O., Ajiboye, T. O., Omotola, E. O., and Oyewola, O. J. (2022). Methylene blue dye: Toxicity and potential elimination technology from wastewater. *Results in Engineering*, 16: 100678.
- Deng, S. Q., Miao, Y. L., Tan, Y. L., Fang, H. N., Li, Y. T., Mo, X. J., Cai, S. L., Fan, J., Zhang, W. G., and Zheng, S. R. (2019). An anionic nanotubular metal-organic framework for highcapacity dye adsorption and dye degradation in darkness. *Inorganic Chemistry*, 58 (20): 13979-13987.
- 8. Lu, L., Shan, R., Shi, Y., Wang, S., and Yuan, H. (2019). A novel TiO₂/biochar composite catalysts for photocatalytic degradation of methyl orange. *Chemosphere*, 222: 391-398.

- 9. Akinyemi, A., Agboola, O., Alagbe, E., and Igbokwe, E. (2024). The role of catalyst in the adsorption of dye: Homogeneous catalyst, heterogeneous catalyst, and advanced catalytic activated carbon, critical review. *Desalination and Water Treatment*, 320: 100780.
- Li, S., Zhang, J., Cao, Y., Yang, Y., Xie, T., and Lin, Y. (2022). Visible light assisted heterogeneous photo-fenton-like degradation of rhodamine B based on the Co-POM/N-TiO₂ composites: Catalyst properties, photogenerated carrier transfer and degradation mechanism. Colloids and Surfaces A: Physicochemical and Engineering Aspects, 648: 129248.
- 11. Rodríguez, M., Bussi, J., and León, M. A. D. (2021). Application of pillared raw clay-base catalysts and natural solar radiation for water decontamination by the photo-fenton process. *Separation and Purification Technology*, 259: 118167.
- Guo, X., Chen, S., Liu, Z., Yang, C., and Chen, W. (2023). Catalytic oxidation of methylene blue by using Ni-Fe bimetallic catalyst/NaClO system: Performance, kinetics, mechanism, and DFT calculations. Separation and Purification Technology, 306: 122162.
- 13. Halfadji, A., Naous, M., Kharroubi, K. N., Belmehdi, F. E. Z., and Rajendrachari, S. (2023). An ultrasonic-assisted synthesis, characterization, and application of nano-Fe₃O₄/TiO₂ as nanocatalyst for the removal of organic dye by likephoto-fenton reactions. *Inorganic Chemistry Communications*, 158: 111686.
- 14. Hu, X., Xie, L., Xu, Z., Liu, S., Tan, X., Qian, R., Zhang, R., Jiang, M., Xie, W., and Tian, W. (2021). Photothermal-enhanced Fenton-like catalytic activity of oxygen-deficient nanotitania for efficient and safe tooth whitening. ACS Applied Materials & Interfaces, 13(30): 35315-35327.
- Keerthana, S., Yuvakkumar, R., Ravi, G., Hong, S. I., Al-Sehemi, A. G., and Velauthapillai, D. (2022). Fabrication of Ce doped TiO₂ for efficient organic pollutants removal from wastewater. *Chemosphere*, 293: 133540.
- Alijani, M., and Ilkhechi, N. N. (2018). Effect of Ni doping on the structural and optical properties of TiO₂ nanoparticles at various concentration and temperature. Silicon, 10(6): 2569-2575.
- 17. Ling, C. M., Ong, S. T., and Lee, S. L. (2025). Recent development of surface-modified titanium dioxide for enhanced oxidation catalytic activity: A short review. *Journal of Alloys and Compounds*, 1037: 182226.
- 18. Mohseni-Salehi, M. S., Taheri-Nassaj, E., and Hosseini-Zori, M. (2018). Effect of dopant (Co, Ni) concentration and hydroxyapatite compositing on photocatalytic activity of titania towards dye degradation. *Journal of Photochemistry and Photobiology A: Chemistry*, 356: 57-70.

- 19. Ling, C. M., Teng, C. C., Hatta, M. H. M., and Lee, S. L. (2021). Tungsten oxide doped titania supported on TUD-C for photocatalytic removal of methylene blue. *Platform: A Journal of Science and Technology*, 4(2): 42-52.
- Koh, P. W., Yuliati, L., and Lee, S. L. (2019). Kinetics and optimization studies of photocatalytic degradation of methylene blue over Cr-doped TiO₂ using response surface methodology. *Iranian Journal of Science and Technology, Transactions A: Science*, 43 (1): 95-103.
- Rodríguez, J. L., and Valenzuela, M. (2022). Nibased catalysts used in heterogeneous catalytic ozonation for organic pollutant degradation: A mini review. *Environmental Science and Pollution Research*, 29(56): 84056-84075.
- 22. Mannaa, M. A., Qasim, K. F., Alshorifi, F. T., El-Bahy, S. M., and Salama, R. S. (2021). Role of NiO nanoparticles in enhancing structure properties of TiO₂ and its applications in photodegradation and hydrogen evolution. ACS Omega, 6(45): 30386-30400.
- 23. Ooi, Y. K., Hussin, F., Yuliati, L., and Lee, S. L. (2019). Comparison study on molybdena-titania supported on TUD-1 and TUD-C synthesized via sol-gel templating method: Properties and catalytic performance in olefins epoxidation. *Materials Research Express*, 6(7): 074001.
- 24. Soekiman, C. N., Miyake, K., Hayashi, Y., Zhu, Y., Ota, M., Al-Jabri, H., Inoue, R., Hirota, Y., Uchida, Y., Tanaka, S., Kong, C. Y., and Nishiyama, N. (2020). Synthesis of titanium silicalite-1 (TS-1) zeolite with high content of Ti by a dry gel conversion method using amorphous TiO₂-SiO₂ composite with highly dispersed Ti species. *Materials Today Chemistry*, 16: 100209.
- Al-Shehri, B. M., Shabaan, M. R., Shkir, M., and Hamdy, M. S. (2020). Single-step fabrication of Na-TUD-1 novel heterogeneous base nanocatalyst for knoevenagel condensation reaction. *Journal of Nanostructure in Chemistry*, 11(2): 259-269.
- Boora, A., Duhan, S., Rohilla, B., Malik, P., Sehrawat, S., Goyat, M., Mishra, Y. K., and Kumar, V. (2024). A three-dimensional ZnO/TUD-1 nanocomposite-based multifunctioal sensor for humidity detection and wastewater remediation. Materials Advances, 5(10): 4467-4479.
- Ekinci, E., Oruç, M., Oktar, N., and Murtezaoğlu, S. (2024). Catalytic performances of Nicontaining mesoporous TUD-1 catalysts in steam reforming of acetic acid. *Catalysis Letters*, 154(7): 3776-3786.
- Zhang, L., Xing, L., Liu, J., Qi, T., Li, M., and Wang, L. (2021). Synchronous catalysis of sulfite oxidation and abatement of Hg²⁺ in wet desulfurization using one-pot synthesized Co-TUD-1/S. Separation and Purification Technology, 266: 118546.

- Alhanash, A. M., Alqahtani, F. A., Aldalbahi, A., Rahaman, M., Benaissa, M., and Hamdy, M. S. (2021). The hydrogenation of cycloalkenes over direct-synthetized well-defined zero-valent Pt nanoparticles incorporated TUD-1 mesoporous material. *Inorganic Chemistry Communications*, 127: 108545.
- Ng, N., Keyon, A. S. A., Ibrahim, W. A. W., Sanagi, M. M., Sutirman, Z. A., and Marsin, F.M. (2023). Amino-functionalised chrysin as adsorbent in dispersive micro-solid phase extraction of selected heavy metal ions from stingless bee honey. *Journal of Food Composition* and Analysis, 123: 105561.
- Dutta, A., Nayak, M., Nag, R., Bera, A., Bhaumik, S., Akhtar, A. J., and Saha, S. K. (2024). Precipitation-assisted, low-temperature-annealed TiO₂ and its nanocomposites-based photoanode for DSSCs. *Journal of Materials Science: Materials in Electronics*, 35(4): 292.
- 32. Keshri, K. S., Bhattacharjae, S., Singha, A., Bhaumik, A., and Chowdhury, B. (2022). Synthesis of cyclic carbonates of different epoxides using CO₂ as a C1 building block over Ag/TUD-1 mesoporous silica catalyst: A solvent free approach. *Molecular Catalysis*, 522: 112234.
- Garg, A., Singhania, T., Singh, A., Sharma, S., Rani, S., Neogy, A., Yadav, S. R., Sangal, V. K., and Garg, N. (2019). Photocatalytic degradation of bisphenol-a using N, Co codoped TiO₂ catalyst under solar light. *Scientific Reports*, 9(1): 765.
- 34. Ballestas-Barrientos, A. R., Xia, Q., Masters, A. F., Ling, C. D., and Maschmeyer, T. (2020). Interfacial reactions between lithium and grain boundaries from anatase TiO₂-TUD-1 electrodes in lithium-ion batteries with enhanced capacity retention. *ACS Omega*, 5(13): 7584-7592.
- Klinyod, S., Yomthong, K., Suttipat, D., Pornsetmetakul, P., Kidkhunthod, P., Choojun, K., Namuangruk, S., Sooknoi, T., and Wattanakit, P. C. (2025). Tailoring the first coordination shell of isolated Ti(IV) active sites in zeolite frameworks boosting catalytic activity in epoxidation. *ChemCatChem*, 17(9): e202401862.
- Ekhsan, J. M., Lee, S. L., and Nur, H. (2014). Niobium oxide and phosphoric acid impregnated silica-titania as oxidative-acidic bifunctional catalyst. *Applied Catalysis A: General*, 471: 142-148.
- Koh, P. W., Leong, C. Y., Yuliati, L., Nur, H., and Lee, S. L. (2020). Role of vanadia and titania phases in the removal of methylene blue by adsorption and photocatalytic degradation. *Malaysian Journal of Analytical Sciences*, 24(6): 1045-1060.
- Ling, C. M., Yuliati, L., Lintang, H. O., and Lee, C. L. (2020). TUD-C supported tungsten oxide doped titania catalysts for cyclohexane oxidation. *Malaysian Journal of Chemistry*, 22(2): 29-36.

- 39. Guettaia, D., Zazoua, H., Bachari, K., and Boudjemaa, A. (2022). A facile fabrication a novel photocatalyst (Fe-TUD-1) with enhanced photocatalytic degradation of ibuprofen. *Reaction Kinetics, Mechanisms and Catalysis*, 135(6): 3359-3374.
- 40. Liu, L., Chen, Z., Zhang, J., Shan, D., Wu, Y., Bai, L., and Wang, B. (2021). Treatment of industrial dye wastewater and pharmaceutical residue wastewater by advanced oxidation processes and its combination with nanocatalysts: A review. *Journal of Water Process Engineering*, 42: 102122.
- Peramune, D., Manatunga, D. C., Dassanayake, R. S., Premalal, V., Liyanage, R. N., Gunathilake, C., and Abidi, N. (2022). Recent advances in biopolymer-based advanced oxidation processes for dye removal applications: A review. *Environmental Research*, 215: 114242.
- 42. Targhan, H., Evans, P., and Bahrami, K. (2021). A review of the role of hydrogen peroxide in organic transformations. *Journal of Industrial and Engineering Chemistry*, 104: 295-332.
- 43. Xue, G., Wang, Q., Qian, Y., Gao, P., Su, Y., Liu, Z., Chen, H., Li, X., and Chen, J. (2019). Simultaneous removal of aniline, antimony and chromium by ZVI coupled with H₂O₂: Implication for textile wastewater treatment. *Journal of Hazardous Materials*, 368: 840-848.
- 44. Liu, Z., Wang, T., Yu, X., Geng, Z., Sang, Y., and Liu, H. (2017). In situ alternative switching between Ti⁴⁺ and Ti³⁺ driven by H₂O₂ in TiO₂ nanostructures: Mechanism of pseudo-fenton reaction. *Materials Chemistry Frontiers*, 1(10): 1989-1994.
- 45. Badvi, K., and Javanbakht, V. (2021). Enhanced photocatalytic degradation of dye contaminants with TiO₂ immobilized on ZSM-5 zeolite modified with nickel nanoparticles. *Journal of Cleaner Production*, 280: 124518.
- 46. Al-Shehri, B. M., Mohamed, S. K., Alzahly, S., and Hamdy, M. S. (2021). A significant improvement in adsorption behavior of mesoporous TUD-1 silica through neodymium incorporation. *Journal of Rare Earths*, 39 (4): 469-476.
- Wang, N., Chen, J., Wang, J., Feng, J., and Yan,
 W. (2019). Removal of methylene blue by polyaniline/TiO₂ hydrate: Adsorption kinetic, isotherm and mechanism studies. *Powder Technology*, 347: 93-102.
- 48. Rajagopal, S., Paramasivam, B., and Muniyasamy, K. (2020). Photocatalytic removal of cationic and anionic dyes in the textile wastewater by H₂O₂ assisted TiO₂ and micro-cellulose composites. Separation and Purification Technology, 252: 117444.

- Tichapondwa, S. M., Newman, J. P., and Kubheka,
 O. (2020). Effect of TiO₂ phase on the photocatalytic degradation of methylene blue dye.
 Physics and Chemistry of the Earth, Parts A/B/C, 118: 102900.
- Wei, X., Wang, Y., Feng, Y., Xie, X., Li, X., and Yang, S. (2019). Different adsorption-degradation behavior of methylene blue and congo red in nanoceria/H₂O₂ system under alkaline conditions. *Scientific Reports*, 9(1): 4964.
- 51. Muthamilarasu, A., Sivakumar, S., Divya, G., Sivakumar, M., and Sakthi, D. (2022). NiO/CuO/TiO₂ ternary composites: Development, physicochemical characterization and photocatalytic degradation study over reactive orange 30 solutions under solar light irradiation. Advances in Materials Science, 22(1): 36-54.
- 52. Somsesta, N., Sricharoenchaikul, V., and Aht-Ong, D. (2020). Adsorption removal of methylene blue onto activated carbon/cellulose biocomposite films: Equilibrium and kinetic studies. *Materials Chemistry and Physics*, 240: 122221.
- 53. Igwegbe, C. A., Mohmmadi, L., Ahmadi, S., Rahdar, A., Khadkhodaiy, D., and Dehghani, R. (2019). Modeling of adsorption of methylene blue dye on Ho-CaWO₄ nanoparticles using response surface methodology (RSM) and Artificial Neural Network (ANN) Techniques. *Methods X*, 6: 1779-1797.
- 54. Priatmoko, S., Widhihastuti, E., Widiarti, N., and Subagja, D. (2021). Synthesis of Ni/NiO-TiO₂ using sol-gel method and its activity in blue methylene degradation. *Journal of Physics: Conference Series*, 1918(3): 032013.
- 55. Mohammed, W., Matalkeh, M., Soubaihi, R. M. A., Elzatahry, A., and Saoud, K. M. (2023). Visible light photocatalytic degradation of methylene blue dye and pharmaceutical wastes over ternary NiO/Ag/TiO₂ heterojunction. ACS Omega, 8(43): 40063-40077.

- Kurokawa, Y., Nguyen, D. T., and Taguchi, K. (2020). Enhancing the photocatalytic activity of commercial P25 TiO₂ powder by combining with handmade Ni-doped TiO₂ powder. *International Journal of Electrical and Computer Engineering*, 10 (2): 1782-1790.
- Gnanasekaran, L., Hemamalini, R., Rajendran, S., Naushad, M., Qin, J., Gracia, F., and Cornejo, L. (2020). Photocatalytic degradation of organic dyes using nickel oxide incorporated titania nanocatalyst. *Desalination and Water Treatment*, 182: 359-364.
- Villamayor, A., Pomone, T., Perero, S., Ferraris, M., Barrio, V. L., G-Berasategui, E., and Kelly, P. (2023). Development of photocatalytic nanostructured TiO₂ and NiO/TiO₂ coatings by DC magnetron sputtering for photocatalytic applications. *Ceramics International*, 49(11): 19309-19317.
- 59. Wiedmer, D., Sagstuen, E., Welch, K., Haugen, H. J., and Tiainen, H. (2016). Oxidative power of aqueous non-irradiated TiO₂-H₂O₂ suspensions: Methylene blue degradation and the role of reactive oxygen species. *Applied Catalysis B: Environmental*, 198: 9-15.
- Vo, Q. V., Thao, L. T. T., Manh, T. D., Bay, M. V., Truong-Le, B. T., Hoa, N. T., and Mechler, A. (2024). Reaction of methylene blue with OH radicals in the aqueous environment: mechanism, kinetics, products and risk assessment. *RSC Advances*, 14(37): 27265-27273.
- 61. Mohammed, K. S., Atlabachew, M., Aragaw, B. A., and Asmare, Z. G. (2024). Synthesis of kaolin-supported nickel oxide composites for the catalytic oxidative degradation of methylene blue dye. *ACS Omega*, 9(4): 4287-4299.
- 62. Pham, V. L., Kim, D. G., and Ko, S. O. (2020). Mechanisms of methylene blue degradation by nano-sized β-MnO₂. *KSCE Journal of Civil Engineering*, 24(5): 1385-1394.